J. Fluid Mech. (1968), *vol.* 34, *part* 4, *pp.* 795–808
Printed in Great Britain

Laminar flow of a stably stratified fluid past a flat plate

By YIH-HO PAO
Boeing Scientific Research Laboratories, Seattle, Washington

(Received 9 November 1967 and in revised form 17 April 1968)

Laminar flow of a stably stratified fluid with uniform upstream velocity and density gradient past a flat plate is investigated experimentally and theoretically. In the experimental study, the flat plate, parallel to the direction of motion, is towed horizontally at uniform speeds in a tank of stratified salt water at uniform density gradients. The horizontal velocity in front of, above, and behind the flat plate is measured with a flow visualization technique. One of the striking phenomena is the strong upstream influence (the upstream wake) of an obstacle in a flow of stably stratified fluid when the gravity effect is comparable to, or more than the inertial effect. The velocity profiles of the upstream wake and boundary layer above the flat plate are wavy and found to be governed by the ratio of Reynolds number Re to Richardson number Ri. The problem is also analysed theoretically with Boussinesq's approximation and two-parameter perturbation expansions for the upstream wake and the boundary layer. The solutions for the upstream wake and for the boundary layer are compared with measurements.

1. Introduction

This study concerns laminar flow past a finite thin flat plate with uniform upstream velocity and density gradient. This problem was first studied by Long (1959, 1962). Long (1959) has demonstrated experimentally the qualitative behaviour of the upstream disturbances caused by a finite flat plate moving in a stratified fluid, and analysed the problem by successive application of the boundary-layer approximation and Stoke's approximation, and obtained a reduced equation. He has obtained a similarity solution for the upstream wake.

Experimentally, we have towed flat plates at uniform speeds in stratified salt water with constant density gradients. The density gradients are measured by single electrode conductivity probes before each run. The streamwise velocity fields in front of, above, and after the flat plate are measured by a flow visualization technique. The experimental apparatus and results will be described in § 2.

Theoretically, we have applied the Boussinesq approximation to the governing equations (§ 3). After assuming the fluid is non-diffusive, two-parameter perturbation expansions are applied. The first-order expansion for the flow field upstream of the flat plate is essentially the same as that obtained by Long (1959). The first-order solution is compared with the upstream wake measure-

ments in §4. The perturbation expansions for the flow field directly above the flat plate are treated in §5. Results from the zeroth order expansion are compared with our measured boundary-layer profiles. This report is the first of a series of experimental and theoretical studies concerning laminar and turbulent flows of stratified fluid past obstacles (Pao 1965, 1967*a–c*; Pao & Timm 1966; Timm & Pao 1966).

2. Experimental apparatus and results

A laminated fibreglass flat plate ($\frac{1}{16}$ in. thick and 16 in. wide) is towed edgewise horizontally at uniform speed in a tank ($9\frac{1}{2}$ ft. × 16 in. × 20 in.) of stratified salt water with uniform density gradient. The plate lengths are 2, 4 and 10 in. long

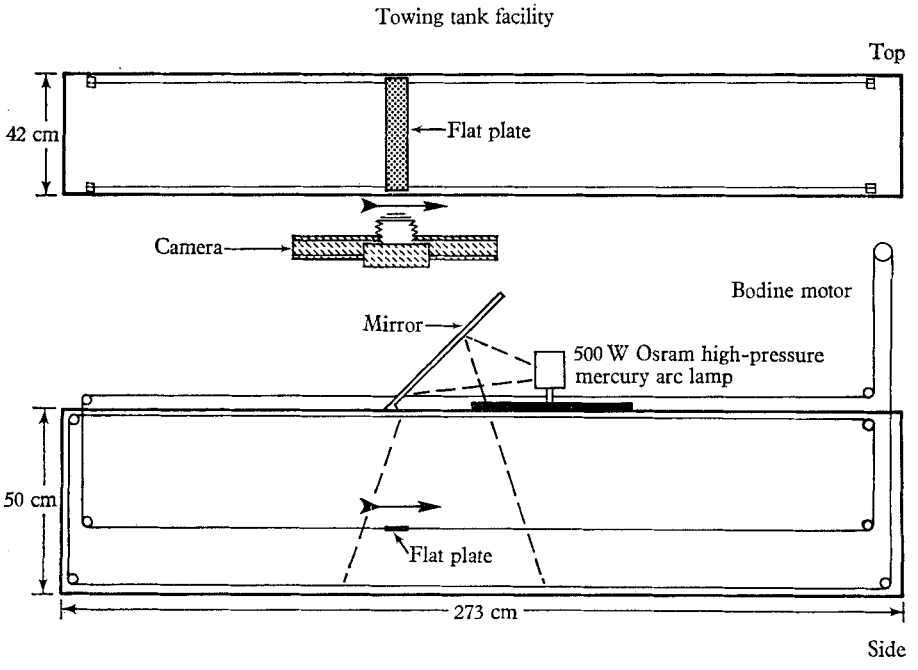

FIGURE 1. Experimental set-up.

respectively. The leading and trailing edges of the plate are streamlined. The depth of stratified salt water is 14 in. The flat plate is towed in the middle of the channel (7 in. from the bottom or the top free surface). The experimental set-up is shown schematically in figure 1. Before each run, the density profile is measured with a single electrode conductivity probe, similar to those developed by Gibson & Schwarz (1963). A typical density profile measurement is shown in figure 2. The flow around the flat plate is made visible with tracers and a bright sheet of light ($\frac{1}{4}$ in. thick and 4 ft. wide). The tracers are neutrally buoyant liquid drops and/or aluminum powder injected into the stratified fluid with a syringe and hypodermic needle. Streak pictures are taken with a Beattie Varitron 70 mm camera moving at the same speed as the plate. The streaks are chopped by a

chopper of known frequency. The horizontal velocities in front of, above, and behind the plate are measured from the chopped streak pictures with the help of a Readex machine. Consecutive streak pictures of the flow field are taken from the start of the plate motion. The steady-state is said to be achieved when the velocity profiles cease to vary from frame to frame.

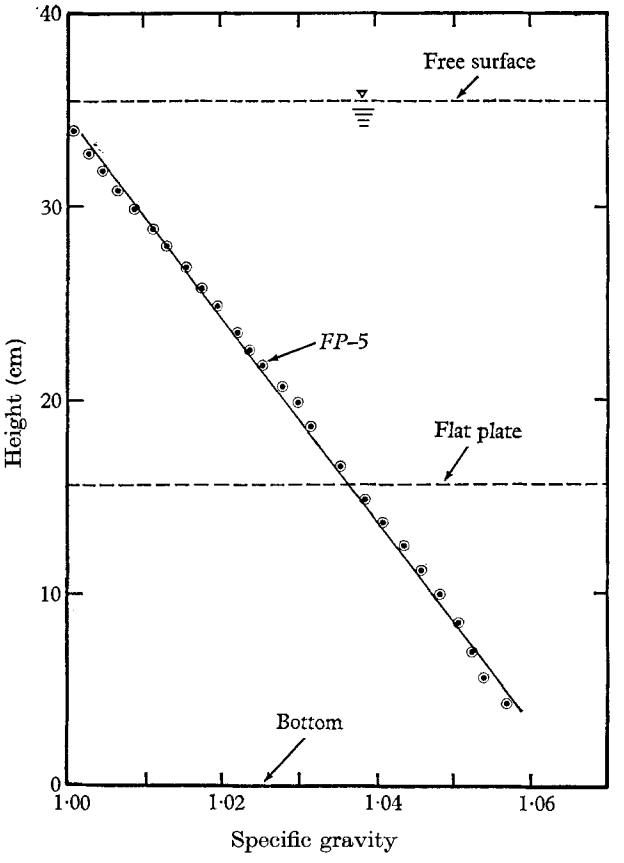

FIGURE 2. A measured density profile.

We have taken care to ensure that our results are not influenced by end walls. A single electrode conductivity probe (with sensitivity to 10^{-5} specific gravity) was inserted at one end of the tank (in front of the plate) before each run. No motion was observed at the end while the data were taken in the middle portion of the tank. We have also taken slow motion pictures (at 8 frames/sec) in front of the plate for a number of runs. When they are shown in the normal 24 frames/sec, the motion is sped up three times, and thus, slow drifting motion is likely to be detected. From these films, we determine the run conditions such that end walls will not affect our measurements.

A total of 16 runs have been made, with plate speeds ranging from 0·163 to 0·975 cm/sec, and with density stratification $\rho_0^{-1}|d\rho/dz|_0$ ranging from 2·93 to $23{\cdot}1 \times 10^{-4}$ cm^{-1}. The Reynolds numbers range from 300 to 1651, and the

Richardson numbers range from 70 to 50,300, where Richardson number Ri is defined as $(g/\rho_0)\ |d\rho/dz|_0 L^2/U^2$ and Reynolds number Re is defined as UL/ν, g is the gravitational acceleration, ρ_0 is the upstream density at the plate level, L is the plate length, U is the constant plate speed, and $|d\rho/dz|_0$ is the absolute value of the uniform upstream density gradient; ν is the kinematic viscosity of the fluid. The details of all runs are listed in table 1 of Pao (1967*b*). The prefix FP indicates flat plate experiments.

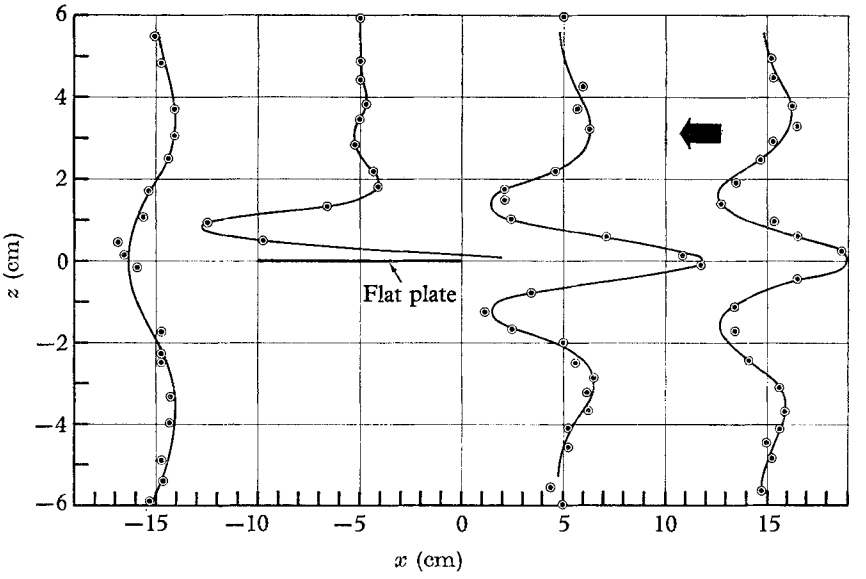

FIGURE 3. Measured horizontal velocity profiles (Re/Ri = 0·201). Run FP–8: Re = 330, Ri = 1640. Scale for velocity $u+U$: 5 cm = 0·1 cm/sec.

It is found that, at any given position, the characteristics of the measured horizontal velocity profile are dependent on the ratio of Reynolds number to Richardson number, Re/Ri. The experimental range of Re/Ri is from 0·00821 to 9·42, as shown in table 1 of Pao (1967*b*). Measured results from three runs, FP–8, FP–5, and FP–10, will be discussed in detail; they are representative of the low, medium and high Re/Ri cases respectively:

(i) $Re/Ri \ll 1$. Measured horizontal velocity profiles of run FP–8 (figure 3): Re/Ri = 0·201, the upstream influence of the flat plate is strong (in terms of $|u+U|/U$). The wavy nature of the velocity profiles is quite pronounced in front of, and directly above, the flat plate. The amplitudes of the wavy $u+U$ profiles diminish very rapidly with height. There is a reverse wake behind the flat plate; this reverse wake is the result of coalescing of the two strong 'jets' adjacent to the flat plate.

(ii) $Re/Ri \sim 1$. Measured horizontal velocity profiles of run FP–5 (figure 4): Re/Ri = 1·42, the upstream influence is weaker. The amplitudes of the wavy $u+U$ profiles decrease more slowly with height; thus the influence of the flat plate is felt at greater vertical distances from the plate. The downstream 'reverse' wake is weaker.

(iii) $Re/Ri \gg 1$. Measured horizontal velocity profiles of run FP–10 (figure 5): $Re/Ri = 9{\cdot}42$, the upstream influence of the flat plate further decreases. The amplitudes of the wavy $u+U$ profiles decrease much more slowly with height; thus, the influence of the flat plate is felt at much greater vertical distance from the plate. The wake at $x = -15$ cm becomes a mixture of 'reverse' wake and ordinary wake.

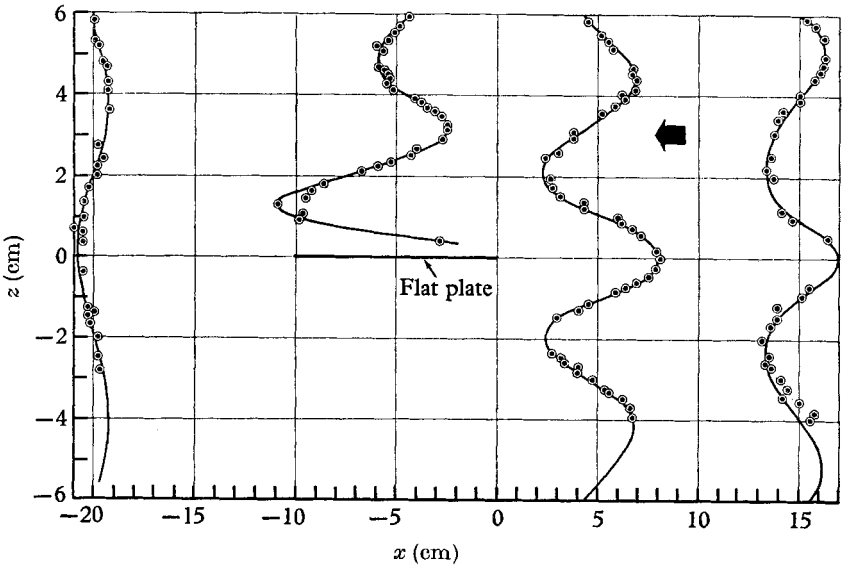

FIGURE 4. Measured horizontal velocity profiles ($Re/Ri = 1{\cdot}42$). Run FP–5; $Re = 660$, $Ri = 466$. Scale for velocity $u+U$: 2 cm = 0·1 cm/sec.

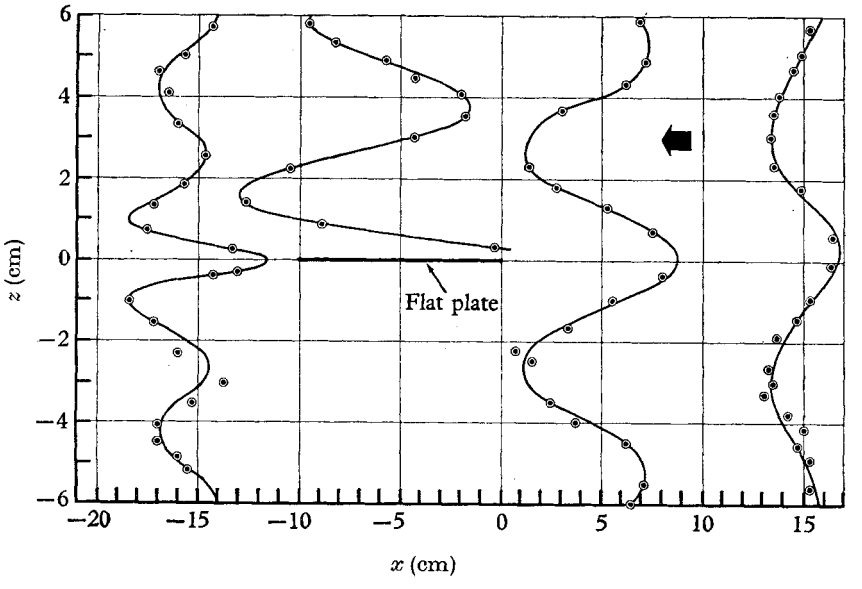

FIGURE 5. Measured horizontal velocity profiles ($Re/Ri = 9{\cdot}39$). Run FP–10, $Re = 991$, $Ri = 106$. Scale for velocity $u+U$: 2 cm = 0·1 cm/sec.

The velocity profiles are outlined with solid lines in figures 3–5. The horizontal velocity measurements of *FP*–8, *FP*–5 and *FP*–10 are tabulated in Pao (1967*b*, table A 1). We have drawn in figures 6 and 7 respectively the non-dimensional

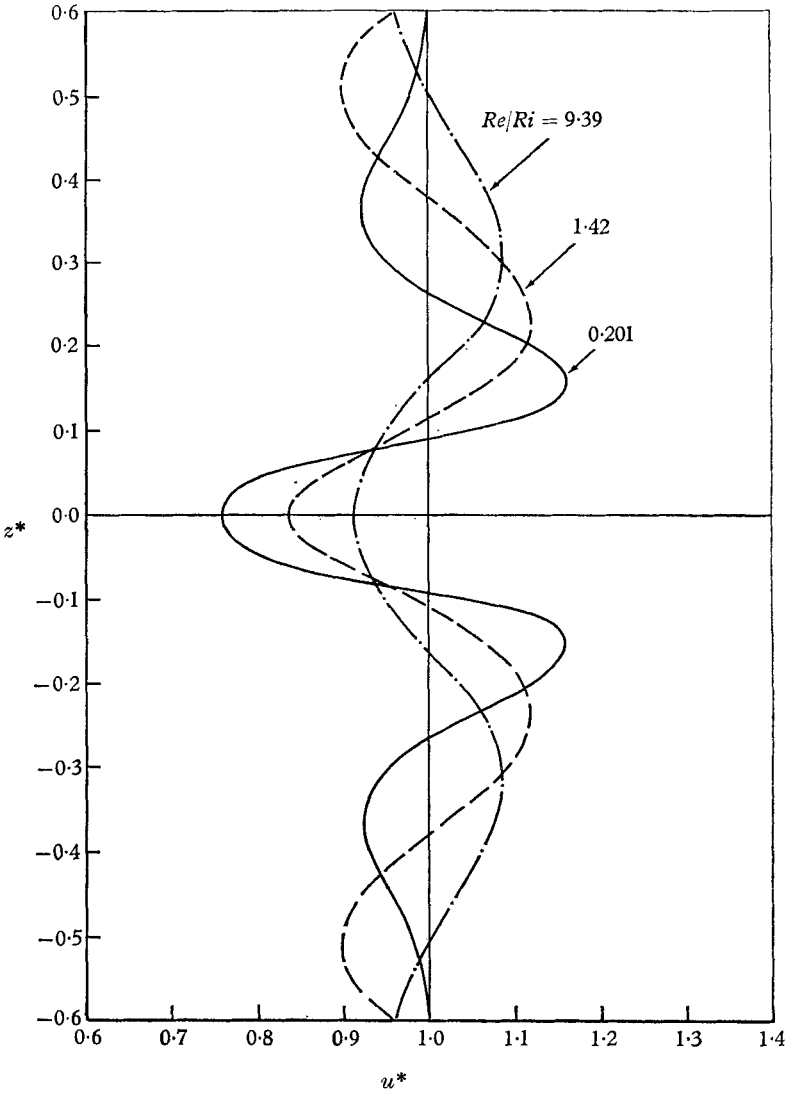

FIGURE 6. The effect of Re/Ri on the upstream wakes. $x/L = 1{\cdot}46$; ———, *FP*–8; – – – –, *FP*–5; —·—·— *FP*–10.

velocity profiles of *FP*–8, *FP*–5 and *FP*–10 in the upstream wakes and in the boundary layers; they show clearly how the velocity profiles vary with Re/Ri.

The measured velocity profiles suggest possible similarity solutions in front of, and directly above, the flat plate, but not behind the flat plate. For more details of the experimental results, see Pao (1967*b*).

3. Governing equations

Assume steady two-dimensional flow of a viscous incompressible, non-diffusive stably stratified fluid with constant viscosity μ; the non-dimensional governing equations with Boussinesq approximation (1903) are

$$\left.\begin{aligned} A(\mathbf{q}^*.\nabla)\mathbf{q}^* &= -\nabla\Lambda^* + \nabla^2\mathbf{q}^* - bs\nabla z^*, \\ \nabla.\mathbf{q}^* &= 0, \quad (\mathbf{q}^*.\nabla)s^* = 0, \end{aligned}\right\} \tag{3.1}$$

where $\mathbf{q}^* = (u^*, w^*) = (uU^{-1}, wU^{-1})$ is the velocity vector. $\Lambda^* = (p + \rho_0 gz)h(U\mu)^{-1}$ is the pressure, $s^* = ss_0^{-1}$ is the reduced salinity, h is an artificial length scale,

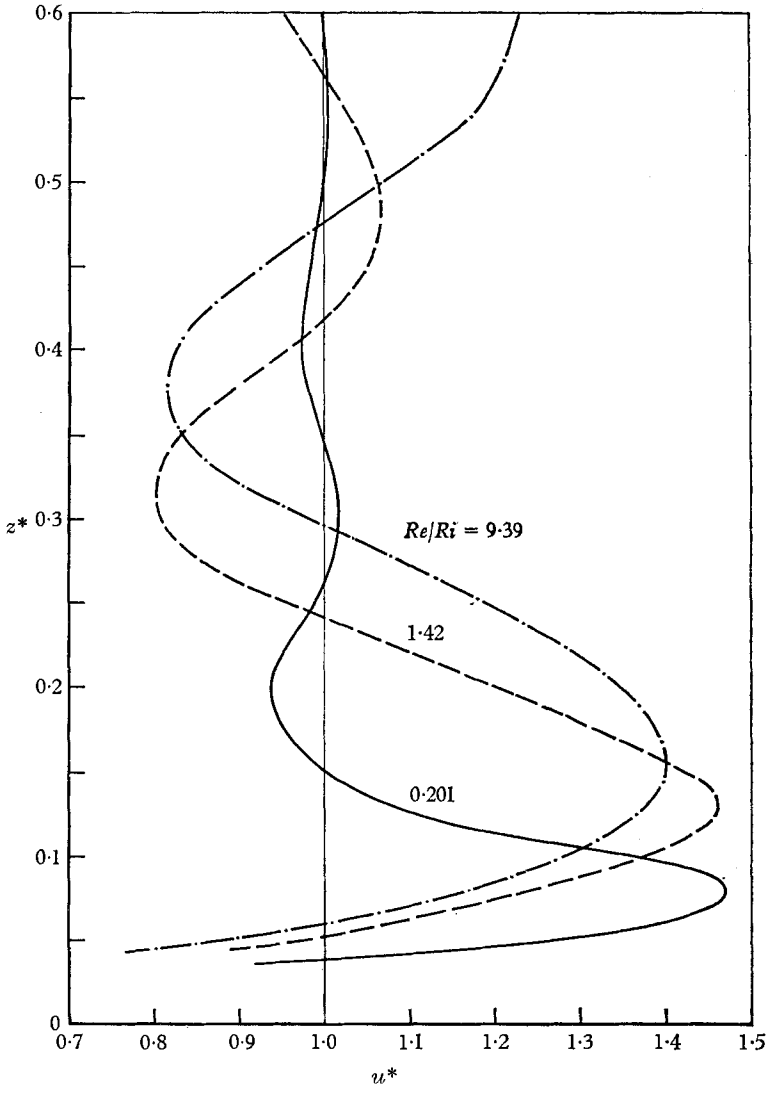

FIGURE 7. The effect of Re/Ri on the boundary layers. $x/L = 0{\cdot}498$; ———, FP-8; – – –, FP-5; —·—·— FP-10.

$A = Uh\rho_0\mu^{-1}$, $b = g\beta h^2U^{-2}$, $x^* = xh^{-1}$ and $z^* = zh^{-1}$ are respectively the horizontal and vertical axes. ρ_0 is a reference density, $|d\rho/dz|_0$ is the constant upstream density gradient, U is the constant upstream velocity, $\beta = (\partial\rho/\partial s)\rho_0^{-1}$.

The non-diffusiveness assumption, $(\mathbf{q}^*.\nabla)s^* = 0$, implies that, for a steady two-dimensional flow, s^* is conserved along any given streamline, i.e. $s^* = s^*(\psi^*)$. The streamfunction ψ^* is related to the velocity field by $u^* = \partial\psi^*/\partial z^*$ and $w^* = -\partial\psi^*/\partial x^*$. It is shown by Long (1959), for a non-diffusive fluid with uniform upstream velocity ($u^* = -1$, $w^* = 0$) and constant upstream density gradient [$\rho_0^{-1}(d\rho/dz)_0 = -k$], (3.1) reduces to

$$\left.\begin{aligned} A(\mathbf{q}^*.\nabla)\mathbf{q}^* &= -\nabla\Lambda^* + \nabla^2\mathbf{q}^* - B\psi^*\nabla z^*, \\ \nabla.\mathbf{q}^* &= 0, \end{aligned}\right\} \tag{3.2}$$

which has two parameters A and B,

$$A = Uh\nu^{-1}, \quad B = gkh^3(U\nu)^{-1}. \tag{3.3}$$

We shall look for perturbation solutions expanded in terms of A and B. The artificial length scale h will be chosen in such a way that both A and B are large and $B > A$. This is possible because $B \sim h^3$ while $A \sim h$.

4. The upstream wake

We shall look for asymptotic solutions of (3.2) for $B \to \infty$ and $\lim_{B\to\infty}(A/B) \to 0$. This expansion scheme is, in principle, analogous to those of Childress (1963), who has investigated the effect of a strong magnetic field on two-dimensional flows of an electrically conducting fluid. Let $B = \epsilon^{-1}$, $A = \epsilon^{-r}$, where $0 < \epsilon \ll 1$, $0 < r < 1$ and r is fixed for a given problem. We shall seek the asymptotic solutions at large distances (compared with h) upstream of the flat plate, i.e. for $x^* = O(\epsilon^{-1})$. Introduce the far-field variables (the tilde indicates the far field variable),

$$\tilde{x} = \epsilon x^*, \quad \tilde{z} = z^*, \quad \tilde{\psi} = \psi^*,$$
$$\tilde{u} = u^*, \quad \tilde{w} = \epsilon^{-1}w^*, \quad \tilde{\Lambda} = \epsilon\Lambda^*.$$

Substituting these variables into (3.2), we obtain

$$\left.\begin{aligned} \epsilon^{(1-r)}\left(\tilde{u}\frac{\partial\tilde{u}}{\partial\tilde{x}} + \tilde{w}\frac{\partial\tilde{u}}{\partial\tilde{z}}\right) &= -\frac{\partial\tilde{\Lambda}}{\partial\tilde{x}} + \epsilon^2\frac{\partial^2\tilde{u}}{\partial\tilde{x}^2} + \frac{\partial^2\tilde{u}}{\partial\tilde{z}^2}, \\ \epsilon^{(3-r)}\left(\tilde{u}\frac{\partial\tilde{w}}{\partial\tilde{x}} + \tilde{w}\frac{\partial\tilde{w}}{\partial\tilde{z}}\right) &= -\frac{\partial\tilde{\Lambda}}{\partial\tilde{z}} + \epsilon^4\frac{\partial^2\tilde{w}}{\partial\tilde{x}^2} + \epsilon^2\frac{\partial^2\tilde{w}}{\partial\tilde{z}^2} - \tilde{\psi}, \\ \frac{\partial\tilde{u}}{\partial\tilde{x}} + \frac{\partial\tilde{w}}{\partial\tilde{z}} &= 0. \end{aligned}\right\} \tag{4.1}$$

The boundary conditions are

$$\text{at infinity:} \quad \tilde{u} = -1, \quad \tilde{w} = 0, \quad \frac{\partial\tilde{u}}{\partial\tilde{z}} = 0;$$

$$\text{on } \tilde{x}\text{-axis:} \quad \frac{\partial\tilde{u}}{\partial\tilde{z}} = \tilde{\psi} = 0 \quad \text{(from symmetry)}.$$

Introduce the perturbation expansions

$$\left.\begin{aligned} \tilde{\psi} &= -\tilde{z}+\epsilon^{(1-r)}\tilde{\psi}_1+\ldots, \quad \tilde{\Lambda} = \tfrac{1}{2}\tilde{z}^2+\epsilon^{(1-r)}\tilde{\Lambda}_1+\ldots, \\ \tilde{u} &= -1+\epsilon^{(1-r)}\tilde{u}_1+\ldots, \quad \tilde{w} = \epsilon^{(1-r)}\tilde{w}_1+\ldots. \end{aligned}\right\} \tag{4.2}$$

Then, the first-order perturbation equation of (4.1) is

$$\left.\begin{aligned} \epsilon^{(1-r)}: \quad 0 &= -\frac{\partial\tilde{\Lambda}_1}{\partial\tilde{x}}+\frac{\partial^2\tilde{u}_1}{\partial\tilde{z}^2}, \quad 0 = -\frac{\partial\tilde{\Lambda}_1}{\partial\tilde{z}}-\tilde{\psi}_1, \\ &\frac{\partial\tilde{u}_1}{\partial\tilde{x}}+\frac{\partial\tilde{w}_1}{\partial\tilde{z}} = 0. \end{aligned}\right\} \tag{4.3}$$

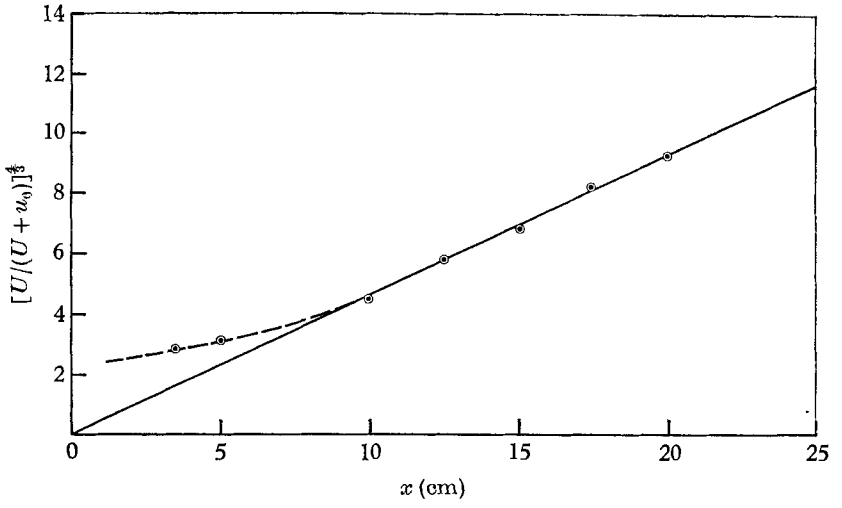

FIGURE 8. Measurements of $[U/(U+u_0)]^{\frac{4}{3}}$ *vs.* x in the upstream wake (*FP*–8).

Assuming similarity solutions of the following form

$$\left.\begin{aligned} \tilde{\psi}_1 &= \tilde{x}^{-\frac{1}{2}}\tilde{F}_1(\tilde{\eta}), \quad \tilde{\Lambda}_1 = \tilde{x}^{-\frac{1}{4}}\tilde{E}_1(\tilde{\eta}), \quad \tilde{\eta} = \tilde{z}\tilde{x}^{-\frac{1}{4}}, \\ \tilde{u}_1 &= \tilde{x}^{-\frac{3}{4}}\tilde{F}'_1(\tilde{\eta}), \quad \tilde{w}_1 = \tfrac{1}{4}\tilde{x}^{-\frac{3}{2}}\{\tilde{\eta}\tilde{F}'_1(\tilde{\eta})+\tilde{F}_1(\tilde{\eta})\}, \end{aligned}\right\} \tag{4.4}$$

(4.3) reduces to a set of ordinary differential equations,

$$4\tilde{F}_1^{\mathrm{iv}}-\tilde{\eta}\tilde{F}'_1-2\tilde{F}_1 = 0, \quad \tilde{E}'_1+\tilde{F}_1 = 0. \tag{4.5}$$

Equation (4.5) was first obtained and solved numerically by Long (1959), and was resolved more accurately by Pao (1967*b*) with a double precision finite difference scheme. Pao (1967*b*) has formulated the perturbation expansions up to the second order (i.e. $\epsilon^{2(1-r)}$ order), and work is under way to solve the higher order approximation. It is clear that for the first-order solution (4.2) to be a valid approximation, all perturbation terms must be small.

Janowitz (1967) has analysed the problem of a point disturbance in a uniform flow of stably stratified fluid with the Oseen approximation. His solution far upstream reduces to (4.5).

We shall compare some experimental results with the first-order solution (4.5). The function $\tilde{F}_1'(\tilde{\eta})/\tilde{F}_1'(0)$ and its higher derivatives have been tabulated in Pao (1967*b*, table A 2). A necessary condition for (4.2) to be a valid approximation is that the expansion parameter $\epsilon^{(1-r)}$ be sufficiently small and $\tilde{x}$ large. Experiment *FP*–8 (see table 1) is chosen for comparison. From (4.2) and (4.4), we obtain

$$\tilde{u}(\tilde{x}, 0) + 1 \cong \epsilon^{(1-r)}\tilde{x}^{-\frac{3}{4}}\tilde{F}_1'(0). \tag{4.6}$$

Equation (4.6) states that the horizontal deficit velocity along the x-axis, $\tilde{u}(\tilde{x}, 0) + 1$, is proportional to $\tilde{x}^{-\frac{3}{4}}$. This serves as a quick check between the first-order theory and experimental results. Measurements of horizontal velocity along the x-axis, $u(x, 0) = u_0$, from *FP*–8 are plotted as $[(U + u_0)/U]^{-4}$ *vs.* x in figure 8.

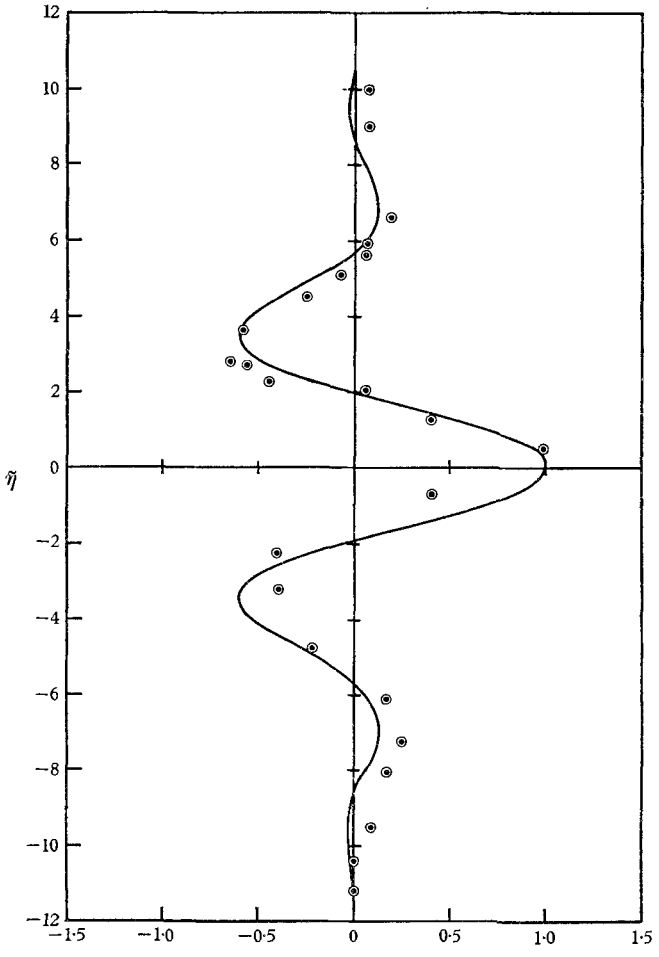

FIGURE 9. The upstream wake, comparing the measured horizontal velocity profile with the theoretical results of a first-order expansion. (Long's solution). (*a*) $(x-x_0)/L = 3{\cdot}15$ (*FP*–8); (*b*) $(x-x_0)/L = 3{\cdot}64$ (*FP*–8). Virtual origin at $x_0/L = -1{\cdot}69$. Leading edge of flat plate at $x = 0$.

The data indeed lie on a straight line for $x > 10$ cm; they agree with the first-order expansion results (4.6). From (4.2), (4.4) and (4.6), we obtain

$$\frac{\tilde{u}+1}{\tilde{u}_0+1} = \frac{\tilde{F}_1'(\tilde{\eta})}{\tilde{F}_1'(0)}. \tag{4.7}$$

This is compared with the upstream velocity profiles measured from run FP–8 ($Re/Ri = 0{\cdot}201$) at two upstream positions in figures 9*a* and 9*b*, respectively, where h is taken to be equal to L. The agreement is fair.

We have compared (4.7) with FP–8 ($Re/Ri = 0{\cdot}201$) at $x/L = 0{\cdot}488$ and they do not agree. This indicates clearly that solution (4.7) is not only restricted to small ϵ, but also to the far field where $x^* = O(\epsilon^{-1})$.

We have also compared (4.7) with FP–3 ($Re/Ri = 0{\cdot}392$) at $x/L = 0{\cdot}492$, 0·984, 1·48, 1·95 and they do not agree.

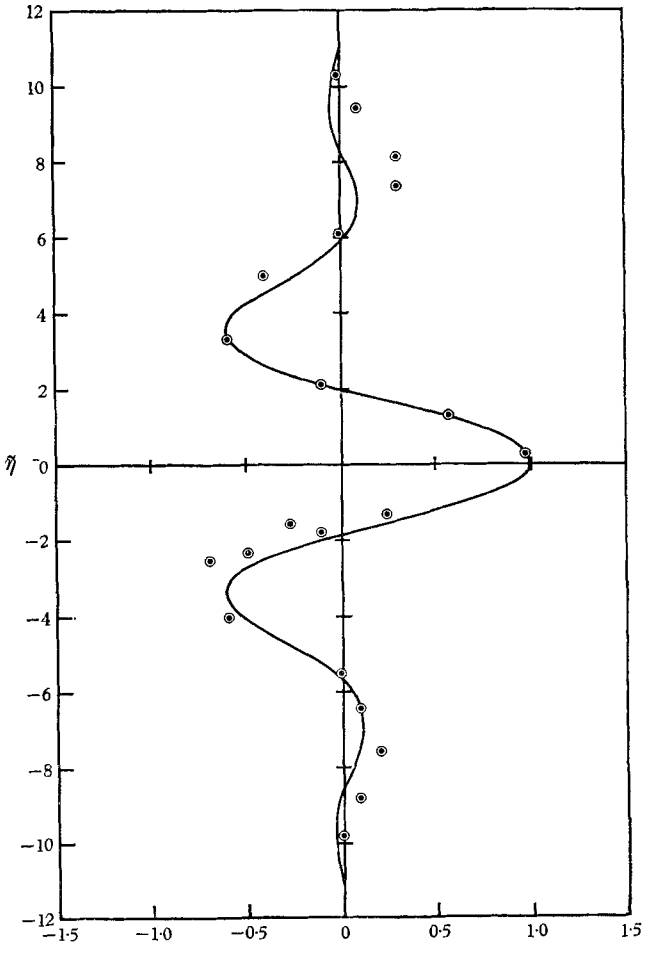

(*b*)

FIGURE 9(*b*). For legend see facing page.

We also find that the experimental results with moderate and large Re/Ri (*FP*–5 and *FP*–10) do not agree with the theoretical results from the far field first-order asymptotic expansion. It is expected that solutions of higher order expansions are needed for these runs.

5. The boundary layer

We shall look for a two-parameter perturbation expansion valid near the flat plate, i.e. for small z^*. Introduce the near field variables (indicated with $^-$)

$$\left.\begin{aligned} &\bar{X} = x^*, \quad \bar{z} = \epsilon^{-\frac{1}{2}} z^*, \quad \bar{\psi} = \epsilon^{-\frac{1}{2}}\psi^*, \\ &\bar{u} = u^*, \quad \bar{w} = \epsilon^{-\frac{1}{2}} w^*, \quad \bar{\Lambda} = \epsilon^{-\frac{1}{2}}\Lambda^*. \end{aligned}\right\} \tag{5.1}$$

Then (3.1) becomes

$$\left.\begin{aligned} \epsilon^{(\frac{1}{2}-r)}\left(\bar{u}\frac{\partial\bar{u}}{\partial\bar{x}} + \bar{w}\frac{\partial\bar{u}}{\partial\bar{z}}\right) &= -\frac{\partial\bar{\Lambda}}{\partial\bar{x}} + \epsilon^{\frac{1}{2}}\frac{\partial^2\bar{u}}{\partial\bar{x}^2} + \frac{\partial^2\bar{u}}{\partial\bar{z}^2}, \\ \epsilon^{(1-r)}\left(\bar{u}\frac{\partial\bar{w}}{\partial\bar{x}} + \bar{w}\frac{\partial\bar{w}}{\partial\bar{z}}\right) &= -\frac{\partial\bar{\Lambda}}{\partial\bar{z}} + \epsilon\frac{\partial^2\bar{w}}{\partial\bar{x}^2} + \epsilon^{\frac{1}{2}}\frac{\partial^2\bar{w}}{\partial\bar{z}^2} - \bar{\psi}. \end{aligned}\right\} \tag{5.2}$$

The boundary conditions are

$$\left.\begin{aligned} &\text{at infinity:} \quad \bar{u} = -1, \bar{w} = 0, \quad \frac{\partial\bar{u}}{\partial\bar{z}} = 0; \\ &\text{on the flat plate} \quad (\bar{z} = 0): \quad \bar{u} = \bar{w} = \bar{\psi} = 0. \end{aligned}\right\} \tag{5.3}$$

Introduce the near-field expansion,

$$\left.\begin{aligned} &\bar{\psi} = \bar{\psi}_0 + \epsilon^{(\frac{1}{2}-r)}\bar{\psi}_1 \ldots, \quad \bar{u} = \bar{u}_0 + \epsilon^{(\frac{1}{2}-r)}\bar{u}_1 + \ldots, \\ &\bar{w} = \bar{w}_0 + \epsilon^{(\frac{1}{2}-r)}\bar{w}_1 + \ldots, \quad \Lambda = \bar{\Lambda}_0 + \epsilon^{(\frac{1}{2}-r)}\bar{\Lambda}_1 + \ldots. \end{aligned}\right\} \tag{5.4}$$

We obtain the governing equations for the zeroth-order expansion

$$\left.\begin{aligned} 0 = -\frac{\partial\bar{\Lambda}_0}{\partial\bar{x}} + \frac{\partial^2\bar{u}_0}{\partial\bar{z}^2}, \quad 0 = -\frac{\partial\bar{\Lambda}_0}{\partial\bar{z}} - \bar{\psi}_0, \\ \frac{\partial\bar{u}_0}{\partial\bar{x}} + \frac{\partial\bar{w}_0}{\partial\bar{z}} = 0. \end{aligned}\right\} \tag{5.5}$$

Let the variables be the following similarity form:

$$\left.\begin{aligned} &\bar{\psi}_0 = \bar{x}^{\frac{1}{4}}\bar{F}_0(\bar{\eta}), \quad \bar{\Lambda}_0 = \bar{x}^{\frac{1}{2}}\bar{E}_0(\bar{\eta}), \\ &\bar{u}_0 = \bar{F}_0'(\bar{\eta}), \quad \bar{w}_0 = \tfrac{1}{4}\bar{x}^{-\frac{3}{4}}(\bar{\eta}\bar{F}_0' - \bar{F}_0), \quad \bar{\eta} = \bar{z}\bar{x}^{-\frac{1}{4}}, \end{aligned}\right\} \tag{5.6}$$

then (5.5) reduces to

$$4\bar{F}_0^{\mathrm{iv}} - \bar{\eta}\bar{F}_0' + \bar{F}_0 = 0, \quad \bar{E}_0' + \bar{F}_0 = 0, \tag{5.7}$$

where $\bar{F}_0(0) = 0$, $\bar{F}_0'(0) = 0$, $\bar{F}_0'(\infty) = -1$, $\bar{F}_0''(\infty) = 0$. Pao (1967*b*) has solved (5.7) numerically with a double precision finite difference method, where the boundary condition at infinity is approximated by $\bar{F}_0'(20) = -1$. The results are tabulated in table A 3 of the same report. Equation (5.4) has also been solved independently by Martin (1966). Pao (1967*b*) has pursued the expansion up to the first-order; work is underway to solve the higher-order approximation numerically.

The zeroth-order solution $\overline{F}'_0$ is compared with the measured horizontal velocity profiles in FP–14 at $x/L = 0{\cdot}803$ and $0{\cdot}212$ in figures 10*a* and *b* respectively. The plate (for FP–14) is 25·4 cm long and 0·159 cm thick. For comparison with the theory, the trailing edge of the plate is placed at the origin; thus the leading edge is at $x/L = 1{\cdot}0$. It is apparent from figure 10 that $\overline{\eta} = \overline{z}/\overline{x}^{\frac{1}{4}}$ is the proper scaling similarity variable for the horizontal velocity profiles above

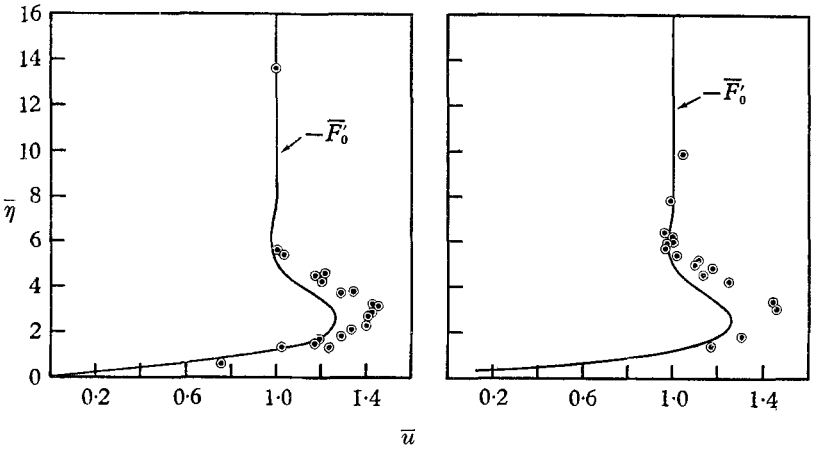

FIGURE 10. The boundary layer, comparing the measured velocity profiles with the theoretical results of a zeroth-order expansion. (*a*) $x/L = 0{\cdot}803$ (FP–14). (*b*) $x/L = 0{\cdot}212$ (FP–14). Trailing edge of flat plate at $x = 0$.

the flat plate. However, the zeroth-order solution $\overline{F}'_0$ underestimates the amplitude of the wavy velocity profiles. Solutions of higher order expansions may improve the situation.

Martin (1966) has independently verified that $\overline{\eta} = \overline{z}/\overline{x}^{\frac{1}{4}}$ is the proper similarity variable for the horizontal velocity profiles above the flat plate by measuring the stagnation surfaces from the streak pictures taken from a stationary camera, although he did not obtain the velocity profiles.

REFERENCES

BOUSSINESQ, J. 1903 *Theorie analytique de la chaleur*, **2**, 172. Paris: Gauthier-Villars.

CHILDRESS, S. 1963 The effect of a strong magnetic field on two-dimensional flows of a conducting fluid. *J. Fluid Mech.* **15**, 429–41.

GIBSON, C. H. & SCHWARZ, W. H. 1963 Detection of conductivity fluctuations in a turbulent flow field. *J. Fluid Mech.* **16**, 357–64.

JANOWITZ, G. S. 1967 On wakes in stratified fluids. Ph.D. Thesis, Department of Mechanics, The Johns Hopkins University.

LONG, R. R. 1959 The motion of fluids with density stratification. *J. Geophys. Res.* **64**, 2151–63.

LONG, R. R. 1962 Velocity concentrations in stratified fluids. *Proc. Am. Soc. Civil Engr., J. Hydraulics Div.* **1**, 9–26.

MARTIN, S. 1966 The slow motion of a finite flat plate through a viscous stratified fluid. Ph.D. Thesis, Department of Mechanics, The Johns Hopkins University.

PAO, Y. H. 1965 Laminar flow of stratified fluid past a flat plate. *Bull. Am. Phys. Soc. Series* 11, **8**, 426.

PAO, Y. H. 1967*a* Turbulence in stratified fluids. Proc. IUGG and IUTAM symposium on boundary layer and turbulence including geophysical applications. *Phys. Fluids*, **10**, S 311.

PAO, Y. H. 1967*b* Laminar flow of a stably stratified fluid past a flat plate. *Boeing Document*, D1–82–0488.

PAO, Y. H. 1967*c* Inviscid flows of stably stratified fluids over barriers. *Boeing Document*, D1–82–0646.

PAO, Y. H. & TIMM, G. K. 1966 Flow of a stratified fluid past a circular cylinder. *Bull. Am. Phys. Soc.* (Series 11), **11**, (5), 721.

TIMM, G. K. & Pao, Y. H. 1966 Laboratory simulation of mountain waves. *Bull. Am. Phys. Soc.* (Series 11), **11** (5), 721.